

A Large-Pulsating-Current Generation and its Application to Identifying Parameters in Jiles-Atherton Model for Current Transformer

Daming Zhang* and Toan Phung

The University of New South Wales, School of Electrical Engineering and Telecommunication
Sydney, NSW, 2052, Australia

*Corresponding author's email: [daming.zhang \[AT\] unsw.edu.au](mailto:daming.zhang@unsw.edu.au)

ABSTRACT— *The purpose of this paper is to present a method for identifying Jiles-Atherton's parameters of current transformer (CT) using differential evolution algorithm and a pulsating current source. The pulse currents are produced from a simple inductor circuit under switched transient. As peak of inrush current can be as high as twenty times its steady-state value and lasts just one to two cycles, such approach has the advantage that it is simple yet it can produce very large current with limited investment to characterize commercial magnetic cored CTs and optical CTs with large current ratings. To illustrate the method of identifying parameters in Jiles-Atherton model using pulse current source, a current transformer with relatively low current rating was used in the experiment. Besides parameters in the Jiles-Atherton model, effective mean length, effective mean cross section and leakage inductance of the CT are also parameters to be identified. Two objective functions were used in the parameter identification, one of which uses the difference of the calculated and measured output currents and the other of which uses the difference of the calculated and measured input currents. With the identified parameters, measured input current is used to predict output current, which is found in good agreement with its measured ones; vice versa, the measured output current is used to predict the input current, which is also found in good agreement with its measured ones. The proposed method is useful in compensation of current transformer, especially under severe fault condition, in which measured current at secondary side is significantly different from its primary side downscaled values. For protection system to operate properly, a proper compensation can be implemented by adapting the proposed method in this paper.*

Keywords— Current transformer, Jiles-Atherton model, Parameter identification, Saturation.

1. INTRODUCTION

Current transformers (CTs) mainly include two types, one being conventional magnetic-cored current transformer and the other being optical current transformer. They can have a wide range of current ratings at the primary side, some of which can be as high as several thousand Amperes. For each of them, the main concern is their capability in linearly duplicating the primary side current, especially up to the saturation point. To test such current transformers up to a meaningful saturation level implies that the test current should be more than twenty times their continuous ratings under normal operation for magnetic cored CT. For example, for a 2000:5 magnetic cored CT, its knee point of saturation current could be as high as 40,000 A. It is a tremendous challenge to produce such high currents as normal laboratories do not have special equipment to do so. In [1], Kucuksari and Karady tried to characterize an optical current transformer with a thermal rating of 3000 A and short-circuit current rating of 63 kA. Maximum current generated in their system is around 4000 A and the current source is bulky and expensive[2-5]. This paper reports the use of inrush current to develop high enough current peaks. The peak of inrush current that occurs in un-magnetized inductors and transformers can be more than twenty times their steady-state values. Since the large inrush pulse just lasts one to two cycles, there is no overheating issue during test. Correspondingly the ratings of equipment used in the test can be lowered. Such inrush currents are pulse-shaped in nature, which is closer to the shape of fault current than sinusoidal current soon after it occurs. By using such inrush current together with a few more turns for the primary side, one can characterize CTs with ratings up to tens of thousands of amperes. In this paper we use the Jiles-Atherton model to characterize a conventional

magnetic-cored CT. A differential evolution method using results from the inrush current data has been adopted to identify Jiles-Atherton parameters for the CT[6-9].

The Jiles-Atherton model and Preisach model are two popular mathematical methods of simulating both the linear and non-linear performance of magnetic cores[10-13]. The advantage of the Jiles-Atherton model is that it can be described by several simple first-order equations, which can be readily incorporated into other equations describing the overall circuit. This paper will demonstrate how the Jiles-Atherton model can be utilized to characterize current transformers.

The differential evolution method is an easy-to-use, reliable and fast global optimizer[14-16]. Once initialized, differential evolution mutates and recombines the population to produce a population of trial vectors. In particular, differential mutation adds a scaled, randomly sampled, vector difference to a third vector. To complement the differential mutation search strategy, differential evolution also employs uniform crossover. Sometimes referred to as discrete recombination, (dual) crossover builds trial vectors out of parameter values that have been copied from two different vectors. If the trial vector has an equal or lower objective function value than that of its target vector, it replaces the target vector in the next generation; otherwise, the target retains its place in the population for at least one more generation. Differential evolution utilizes a set of objective functions in the optimization process. In this paper we use effective objective function for the differential evolution and use it to identify the parameters in the Jiles-Atherton model for a current transformer.

As the measured input and output currents contain noises which make the parameters extraction impossible, a wavelet de-noising method has been introduced to remove the noise.

The paper is organized as follows: In Section II, the Jiles-Atherton model is reviewed; In Section III, the circuit that produces high inrush current is introduced; Section IV describes the wavelet de-noising method to remove noise in the measured input and output currents of the current transformer under test; Section V presents differential evolution method to extract parameters in the Jiles-Atherton model. Section VI concludes the paper.

2. THE JILES-ATHERTON MODEL TO IDENTIFICATION OF PARAMETERS FOR CURRENT TRANSFORMERS

2.1 Current transformer representation using the Jiles-Atherton Model[10-13]

The non-linearity of the current transformer core is modelled using the Jiles-Atherton model as shown in Fig.1. As copper resistance and leakage reactance of the primary side have no influence on the CT performance, they are ignored in the equivalent circuit as shown in Fig. 1. But their counterparts in the secondary side do have influence. The copper resistance of CT at the secondary side under study was measured and is equal to 1.2 Ω. It is lumped with burden resistance. As it is impossible to separate the leakage inductance for either side, the leakage inductance L as indicated in Fig. 1 of the secondary side is left to be identified.

The basic equations for the current transformer in Fig. 1 are given by

$$i_2(t) = i_1(t) / N \quad (1)$$

$$i_2(t) = i_{m2}(t) + i_L(t) \quad (2)$$

$$v_m(t) = i_L(t) \cdot R + L \frac{di_L(t)}{dt} \quad (3)$$

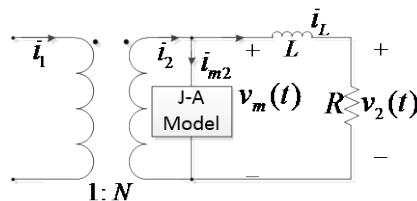


Figure 1: The current transformer model combining an ideal 1:N transformer model and a magnetizing branch modeled using a Jiles-Atherton model to capture non-linear and hysteresis effects.

2.2 Jiles-Atherton Model

A review of the dynamic Jiles-Atherton model [10-14] is provided in this section. The derivative of the irreversible magnetization against magnetic field intensity is given by:

$$\frac{dM_{irr}}{dH} = \frac{M_{an}(H_e) - M_{irr}}{k \cdot \text{sign}\left(\frac{dH}{dt}\right) - \alpha [M_{an}(H_e) - M_{irr}]} \quad (4)$$

where M_{irr} is the irreversible magnetization, M_{an} is the anhysteretic magnetization, $sign$ is defined as $sign(x) = 1$ for $x \geq 0$ and $sign(x) = -1$ for $x < 0$. The reversible magnetization, M_{rev} , is

$$\frac{dM_{rev}}{dH} = c \left(\frac{dM_{an}}{dH} - \frac{dM}{dH} \right) \quad (5)$$

where M is the total magnetization, and c is the coefficient of proportionality (a Jiles-Atherton parameter). The total magnetization is

$$M = M_{irr} + M_{rev} \quad (6)$$

H_e in (4) is the effective magnetic field which is expressed as

$$H_e = H + \alpha \cdot M \quad (7)$$

where H is the magnetic field in the core, α is the inter-domain coupling factor (a Jiles-Atherton parameter). The flux density, B , is given by

$$B = \mu_0(H + M) \quad (8)$$

where H is the magnetic field or magnetizing field, and μ_0 is the permeability of free space.

The anhysteretic magnetization M_{an} is described using the Langevin function:

$$M_{an} = M_s \left(\coth \frac{H_e}{a} - \frac{a}{H_e} \right) \quad (9)$$

$$\frac{\partial M_{an}}{\partial H} = \frac{M_s}{a} \left[1 - \coth^2 \left(\frac{H_e}{a} \right) + \left(\frac{a}{H_e} \right)^2 \right] \quad (10)$$

where M_s is the saturation magnetic moment of the core material and a is a shape parameter; both Jiles-Atherton parameters.

Using (4)-(10), the following is derived

$$M_{rev} = c(M_{an} - M) \quad (11)$$

$$\frac{dM}{dH} = \frac{1}{1 + c \operatorname{sign}(\dot{H}) * k - \alpha(M_{an} - M_{irr})} + \frac{c}{1 + c} \frac{dM_{an}}{dH} \quad (12)$$

where $M_{an} - M_{irr}$ can then be expressed as $(1+c)(M_{an} - M)$ and k corresponds to hysteresis loss and is expressed as $k_0 + k_1 e^{-H^2/(2\sigma^2)}$ with three parameters k_0, k_1, σ to be identified.

When using the equation $M_{rev} = c(M_{an} - M_{irr})$ instead of (11), one can come to the following expression for computing the derivative of M with H :

$$\frac{dM}{dH} = (1-c) \delta \frac{M_{an} - M}{\operatorname{sign}(\dot{H})k(1-c) - \alpha(M_{an} - M)} + c \cdot \frac{dM_{an}}{dH} \quad (13)$$

where

$$\delta = \begin{cases} 0, & \text{if } \operatorname{sign}(\dot{H}) \times (M_{an} - M) \leq 0 \\ 1, & \text{otherwise} \end{cases} \quad (14)$$

In (13), the coefficient δ is introduced as for line segments ab and cd in Fig. 2, all magnetization is reversible, and $\delta=0$ for these two segments and $M_{irr}=0$ and $M_{rev}=cM_{an}$.

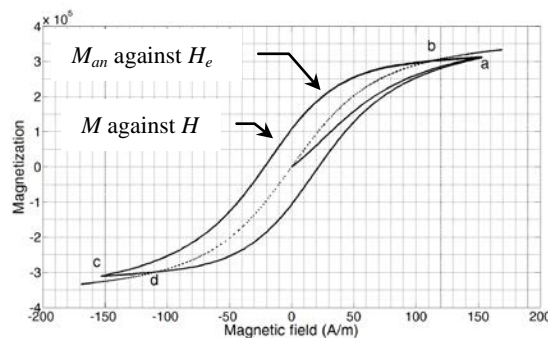


Figure 2: Magnetization curves: Solid - Magnetization against magnetic field; Dotted - Anhysteretic magnetization against magnetic field

2.3 Computation of current transformer output current with a known Load Resistance and Primary Side Current

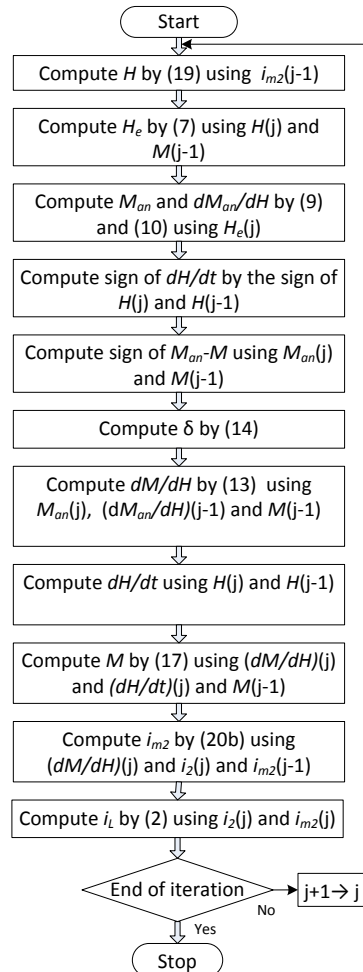


Figure 3: Flowchart for computing i_{m2} , i_L and v_2 with given i_2

From Fig.1 the voltage across the Jiles-Atherton model is the magnetizing voltage:

$$v_m(t) = R(i_2 - i_{m2}) + Ld(i_2 - i_{m2}) / dt \quad (15)$$

From Faraday's law, one has

$$v_m(t) = N \frac{d\phi}{dt} = \mu_0 NA \frac{d(H + M)}{dt} \quad (16)$$

Since

$$\frac{dM}{dt} = \frac{dM}{dH} \cdot \frac{dH}{dt} \quad (17)$$

Then

$$v_m(t) = \mu_0 NA \cdot \left(1 + \frac{dM}{dH} \right) \cdot \frac{dH}{dt} \quad (18)$$

where A is the cross sectional area of the core and N is the number of turns at secondary side of current transformer. The primary side of current transformer is assumed to have one turn.

The current transformer core is assumed to be a toroid with an average diameter of D and an average circumference of l . Thus

$$H = \frac{Ni_{m2}}{\pi D} \quad (19)$$

From (15), (18) and (19) we get

$$\frac{di_{m2}}{dt} = \frac{\pi D}{\mu_0 N^2 A} \cdot \frac{1}{1 + dM / dH} \cdot v_m(t) \quad (20a)$$

Or, discretised,

$$\frac{i_{m2}(j+1) - i_{m2}(j)}{\Delta t} = \frac{\pi D / (\mu_0 N^2 A)}{1 + dM / dH} \cdot v_m(t) \quad (20b)$$

By solving (20b), one can work out i_{m2} then (15) computes the voltage v_2 across the load. The detailed steps for computing i_{m2} , i_L and v_L with a given i_2 are shown in Fig. 3.

2.4 Computation of Magnetizing Current i_{m2} from a known Load Current and Load Resistance

In a practical system, $i_L(t)$ in Fig.1 is usually measured. In this section, we assume that $i_L(t)$ and R are known. In our case, R is a combination of internal copper resistance at secondary side of CT and burden.

Compared with conventional Jiles-Atherton model described in Section II.B, inverse Jiles-Atherton model is more suitable for computing magnetizing current with known magnetizing voltage. In this part load information and load current are known, from which one can compute the magnetizing voltage $v_m(t)$. Hence inverse Jiles-Atherton model is adopted to work out magnetizing current $i_m(t)$, then input current $i_2(t)$.

The inverse Jiles-Atherton model can be described as follows:

$$\frac{dM}{dB} = \begin{cases} \frac{\xi}{\mu_0 [1 + (1 - \alpha)\xi]} & \text{if } \delta_M = 0 \\ \frac{\eta}{\mu_0 [k \cdot \delta + (1 - \alpha)\eta]} & \text{if } \delta_M = 1 \end{cases} \quad (21)$$

where

$$\delta_M = \begin{cases} 0 & \text{if } \text{sign}(dH / dt) \cdot \text{sign}(M_{an} - M) < 0 \\ 1 & \text{if } \text{sign}(dH / dt) \cdot \text{sign}(M_{an} - M) > 0 \end{cases}, \quad (22)$$

$$\xi = c \frac{dM_{an}}{dH_e}, \quad (23)$$

$$\eta = (M_{an} - M) + k \cdot c \cdot \delta \cdot \frac{dM_{an}}{dH_e} \quad (24)$$

and

$$\delta = \begin{cases} 1 & \text{if } \text{sign}(dB / dt) > 0 \\ -1 & \text{if } \text{sign}(dB / dt) < 0 \end{cases} \quad (25)$$

$$v_m(t) = N \frac{d\varphi}{dt} = NA \frac{dB}{dt} \quad (26)$$

$$B(t) = \frac{1}{NA} \int v_m(t) dt \quad (27)$$

$$M(t) = \frac{1}{\mu_0 NA} \int v_m(t) dt - H(t) \quad (28)$$

(19) can be further written as (29)

$$Ni_{m2} = H \cdot (\pi D) \quad (29)$$

$$\frac{dH}{dB} = \frac{1}{\mu_0} \frac{dM}{dB} \quad (30)$$

$$\frac{dH}{dt} = \frac{dB}{dt} \cdot \frac{dH}{dB} = \frac{v_m(t)}{NA} \cdot \frac{dH}{dB} \quad (31)$$

$$dB / dH = 1 / (dH / dB) \quad (32)$$

Eqn. (28) can be discretized as

$$M(j+1) = \sum_{k=1}^{j+1} \frac{v_m(k)}{\mu_0 nA} \times \Delta t - H(j) + M_0 \quad (33a)$$

From the summation in (33a)

$$\text{SumMH}(j+1) = \text{SumMH}(j) + v_m(j+1) \times \Delta t / (\mu_0 NA) \quad (33b)$$

Then

$$M(j+1) = \text{SumMH}(j+1) - H(j) \quad (33c)$$

Eqn. (31) can be discretized as

$$H(j+1) = H(j) + v_m(j+1) \cdot (dH / dB)(j+1) / (NA) \quad (34)$$

Equation (32) can be discretized as

$$B(j+1) = B(j) + \left[1 / (dH / dB)(j+1) \right] \cdot [H(j+1) - H(j)] \quad (35)$$

The flowchart for implementing this computation is shown in detail in Fig. 4 where the magnetizing voltage $v_m(t)$ is treated as known. This is possible as the load current serves as known input to this subroutine.

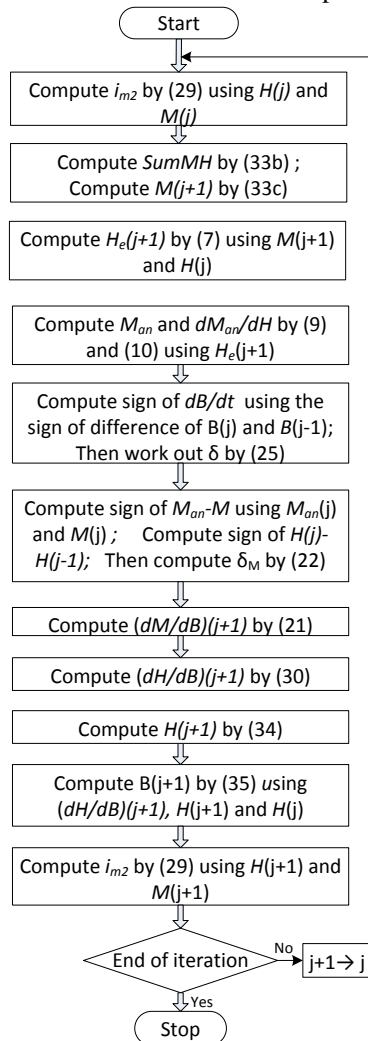


Figure 4: Flowchart for computing i_{m2} and i_2 with known v_2 or i_L

From Sections 2.2, 2.3 and 2.4, one can see that there are ten unknowns: a , α , c , K_b , K_L , σ , M_s , mean length l and mean cross sectional area A . As the CT under test is sealed in resin, its core dimensions are unknown and so the authors put them as parameters to be identified as well. In Section IV we will use differential evolution algorithm to identify all these parameters.

3. INRUSH CURRENT GENERATION FOR CHARACTERIZATION OF CURRENT TRANSFORMER

Figure 5 shows the circuit that is to generate large pulse current. It consists of variable single-phase transformer, fixed ratio transformer of 240V/18V, point-of-wave switch, inductor L1 of 5.5mH and the current transformer under test. As the secondary side of conventional variac transformer can only take up to several amperes which is well less than the inrush current under test, a 240V/18V transformer is adopted whose secondary side could allow several hundred amperes current to flow.

The current transformer under test has the parameters as follows:

- Primary side turns 20; secondary side turns 300;
- Power rating: 2.5 VA;
- Rated current at secondary side: 1 A;
- Rated current at primary side: 15 A.
- Class: 1.0

The current transformer adopted here for study is a measuring current transformer instead of a protective current transformer and its rated current at the secondary side of CT is 1 A. The common working current range for such current transformer is up to around 120% of its rated current, beyond which the core presents saturation effect. The current at the secondary side during measurement is as high as several amperes, which is able to saturate the CT with a proper burden.

Although the method developed here is for characterizing the measuring current transformer, it can be applied for characterizing protective current transformers as well.

Corresponding experiment setup is shown in Fig. 6, where two current probes and a high-precision oscilloscope are used to measure primary and secondary currents. The oscilloscope is Lecroy Wwave Surfer 44MXs-B, which has a maximum sampling rate of 5 GS/s and a vertical accuracy of being better than $\pm 1\%$.

The two current probes used in the experiment are LEM PR30 and PR430. LEM PR30 has a accuracy level of $\pm 1\%$ of reading $\pm 2\text{mA}$ and its frequency response range is from DC to 100kHz. LEM PR430 has a accuracy level of $\pm 1\%$ of reading and its frequency response range is from DC to 20kHz. LEM PR20 can measure current as high as $\pm 30\text{A}$ with the specified accuracy while LEM PR430 can measure current as high as $\pm 400\text{A}$ with its specified accuracy. Such measurement ranges are sufficient for the measurement done in this paper as the current at the secondary side of CT is only several amperes and the current at the primary side of CT is less than ± 200 amperes. Furthermore the frequency components of the currents are well less than 20kHz. Hence the chosen two current probes can satisfy the accuracy requirement of measurement.

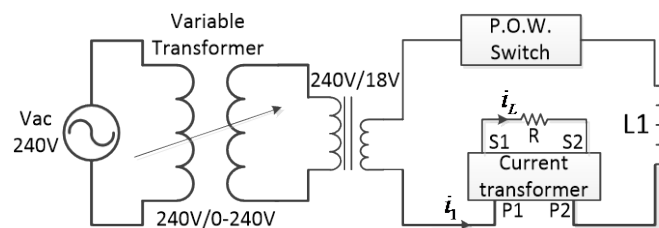


Figure 5: Experimental circuit for large pulse current generation

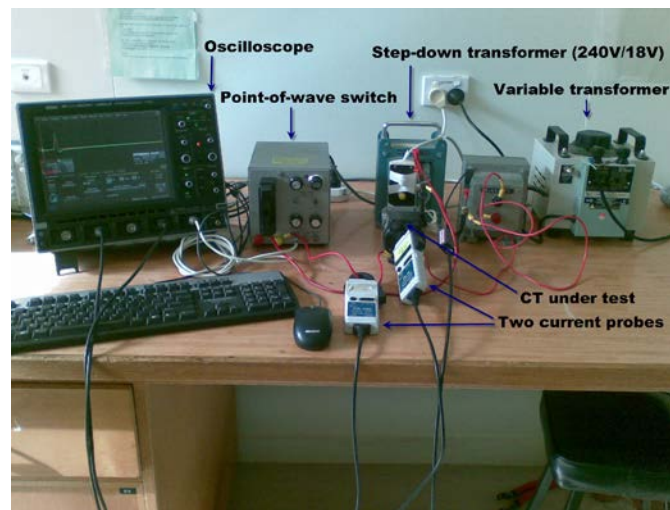


Figure 6: Experimental setup for CT characterization

Assume that the voltage across the secondary side of fixed-turn transformer (240V/18V) is $v(t) = \sqrt{2}V \sin \omega t$ in Fig. 5. If we neglect the core losses and the winding resistance, the flux in the inductor L1 in the circuit can be deduced as follows,

$$\Phi = \frac{1}{N} \int_{t_0}^t v(t) dt = -\frac{\sqrt{2}V}{\omega N} [\cos \omega t - \cos \omega t_0] \quad (36)$$

where t_0 is power-turn-on moment by pressing point-of-wave switch.

If the inductor is powered when the source voltage is at peak or $\omega t_0 = \pi / 2$, then

$$\Phi(t) = -\frac{\sqrt{2}V}{\omega N} [\cos \omega t - \cos \omega t_0] = -\frac{\sqrt{2}V}{\omega N} \cos \omega t . \quad (37)$$

For this case, there is no inrush current that flows and the system is in steady state from the start.

If the inductor is magnetized when the source voltage is at zero or $\omega t_0 = 0$, then

$$\Phi(t) = -\frac{\sqrt{2}V}{\omega N} [\cos \omega t - \cos \omega t_0] = \Phi_m (1 - \cos \omega t). \quad (38)$$

The peak flux has doubled and the corresponding peak magnetizing current can be very large because of core saturation.

By using the Jiles-Atherton model described in Section II, such phenomenon of inrush current can be modelled in Simulink. The diagram of Simulink implementation is shown in Fig. 7, where the non-linear inductor model is shown in the rectangular box with symbol of L. Figure 8 shows one case of simulated maximum inrush current.

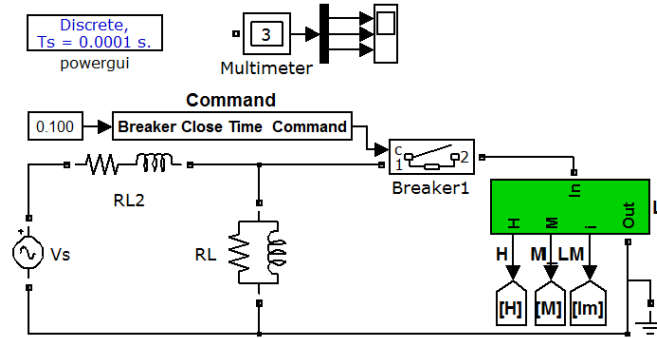


Figure 7: Modelling of inrush current using Simulink

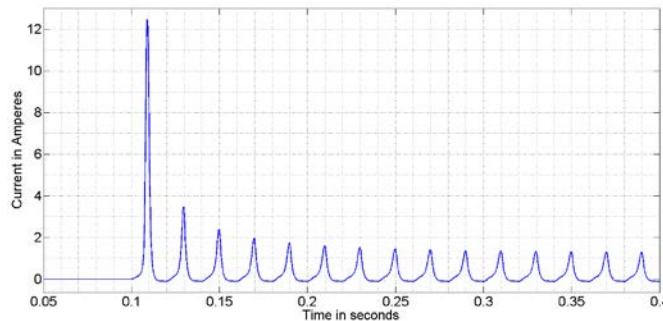


Figure 8: Modelling of inrush current i_l generated in the circuit in Fig.5

4. MEASUREMENT OF CURRENTS OF PRIMARY AND SECONDARY SIDES OF A CURRENT TRANSFORMER AND THEIR DENOISING USING WAVELET TRANSFORM

As shown in Fig. 6, a large inrush current generation circuit was built in our laboratory. Current transformer is connected as shown in the figure with large pulse current i_l flowing through its primary side as indicated by P1 and P2. Its secondary side current is indicated as i_L flowing through the burden, a pure resistor with variable values. The measured currents i_l and i_L contain noise which makes them not suitable for extraction of parameters in the Jiles-Atherton model. Hence a de-noising technique, wavelet analysis was used in this paper to remove the noise.

Wavelet analysis is a signal processing method in time-frequency domain. Similar to Fourier transforms which generate the projection of signal in frequency domain, wavelet analysis is the projection in time-frequency domain. It is an approximation of original signal by linear combination of wavelets.

Wavelet analysis has been widely used in many engineering fields, such as fault detection, image processing, chemical signal analysis, and so on. Generally, the wavelet de-noising procedure involves three steps[16-18]:

1) Decomposition. Wavelet transform is used here to decompose the polluted signal. Transform method, wavelet base and decomposing level are selected.

2) Thresholding. Threshold is chosen to be applied on all detail coefficients.

3) Reconstruction. To reconstruct signal by original approximate coefficients and all modified detail coefficients.

Multi-resolution analysis was adopted in the decomposition in our case. Multi-resolution analysis is a type of discrete wavelet transform using series of filter pairs. Each filter pair divides signal into high and low frequency band which are also called detail and approximate parts, respectively. The fundamental of multi-resolution is shown in Fig. 9 where f is the original signal, A and D stand for approximations and details respectively. The approximate coefficients with lowest frequency (A_3) will be kept in order to reconstruct de-noised signal with modified D_1 , D_2 , and D_3 .

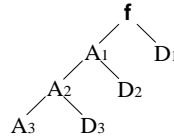


Figure 9: Fundamental of multi-resolution analysis

In our analysis Debauchy 16 with a level of 12 was adopted to de-noise the measured primary and secondary side currents. Figures 10 and 11 show a set of noised and de-noised input and output currents.

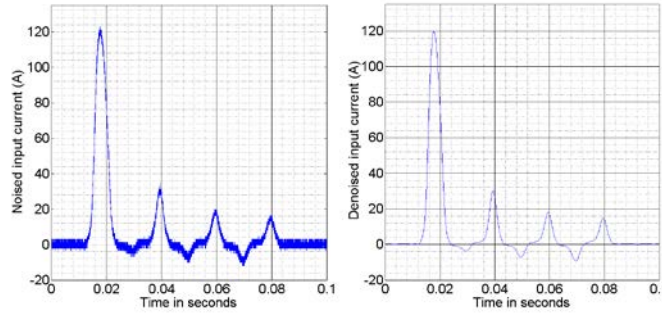


Figure 10: Noised and de-noised input current i_l with a burden of 1.2 Ω

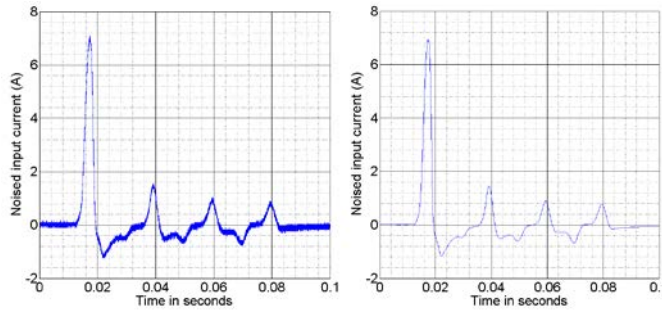


Figure 11: Noised and de-noised output current i_L with a burden of 1.2 Ω

5. PARAMETERS' EXTRACTION USING DIFFERENTIAL EVOLUTION METHOD

The objective functions are calculated from the difference of measured and calculated magnetizing currents.

$$Obj_1 = \sqrt{\frac{\sum_{j=1}^N [i_{mm1}(j) - i_{mc1}(j)]^2}{N}} \quad (39)$$

$$Obj_2 = \sqrt{\frac{\sum_{j=1}^N [i_{mm1}(j) - i_{mc2}(j)]^2}{N}} \quad (40)$$

where i_{mm1} is the difference between i_2 , the measured primary side current referred to the secondary side and the measured secondary current i_L as shown in Fig. 1; i_{mc1} is the difference between the measured i_2 and calculated output current i_L with known i_l by using the method in Section II.C; i_{mc2} is the difference between the calculated i_2 with known load current i_L by using the method in Section II.D and the measured load current i_L .

Figure 12 shows the flowchart for using differential evolution to identify all ten parameters. Figure 12(a) is the main program flowchart, in which de-noised signals are loaded and algorithm of differential evolution is called. Figure 12(b) is the Flowchart of differential evolution algorithm, where the objective function is called. Figure 12(c) is flowchart of subroutine of objective functions.

Table I shows (a) lower and upper limits of Jiles-Atherton parameters with reference to [10] and (b) limits on dimensional parameters. Although the dimensions are unknown for the CT under test, approximate ranges for them are estimated, where the range of leakage inductance for the secondary side is also given. The total leakage inductance referred to secondary side was measured by short-circuiting primary side. The measured total leakage inductance is 21 mH. This CT under study is manufactured by a non-commercial company and does not incorporate means of containing leakage inductance as in conventional commercial CTs. Hence its leakage inductance is large.

To identify all the parameters listed in Table I, one needs to use properly-considered input and output currents. For example, if currents lead to negligible magnetization, then there is no possibility of identifying the ten parameters as the input to output ratio will simply be the turns ratio, 15, and the magnetizing current is almost zero percent of burden current. If the current causes deep saturation, then it is also difficult to obtain accurate values of ten parameters as the

Jiles-Atherton model does not work well under heavy saturation. The suitable values for parameter identification fall in such range that magnetizing current is from 10% to 30% of burden current. By following this criterion, one set of measured values has been adopted to identify the ten parameters.

Measured values shown in Figs. 13 and 14 are the input and output currents used in the parameter identification. The identified values of ten parameters are shown in Table II. By using the identified parameters and following procedures given in Fig. 3, with given measured input current as shown in Fig. 13, the output current is calculated and shown in Fig. 13, from which one can see that they agree with each other very well. In a similar way, by using the identified parameters and following procedures given in Fig. 4, with the measured output current as shown in Fig. 13, the input current is calculated and shown in Fig. 14, from which one can see that it agrees well with the measured input values.

Table1A: Lower and upper limit of parameters in J-A model

| Parameter | a A/m | α 1E-3 | c | K_0 A/m | K_1 A/m | σ | M_s kA/m |
|-------------|------------|------------------|-----|--------------|--------------|----------|---------------|
| Lower limit | 100 | 0.10 | 0.1 | 100 | 10 | 10 | 1000 |
| Upper limit | 2000 | 20 | 1.5 | 2000 | 2000 | 2000 | 1600 |

Table1B: Lower and upper limit of parameters for dimensions and leakage inductance

| Parameter | Mean length (cm) | Mean cross section (cm ²) | Leakage inductance (mH) |
|-------------|---------------------|--|----------------------------|
| Lower limit | 5.0 | 4.0 | 10 |
| Upper limit | 7.5 | 8.0 | 20 |

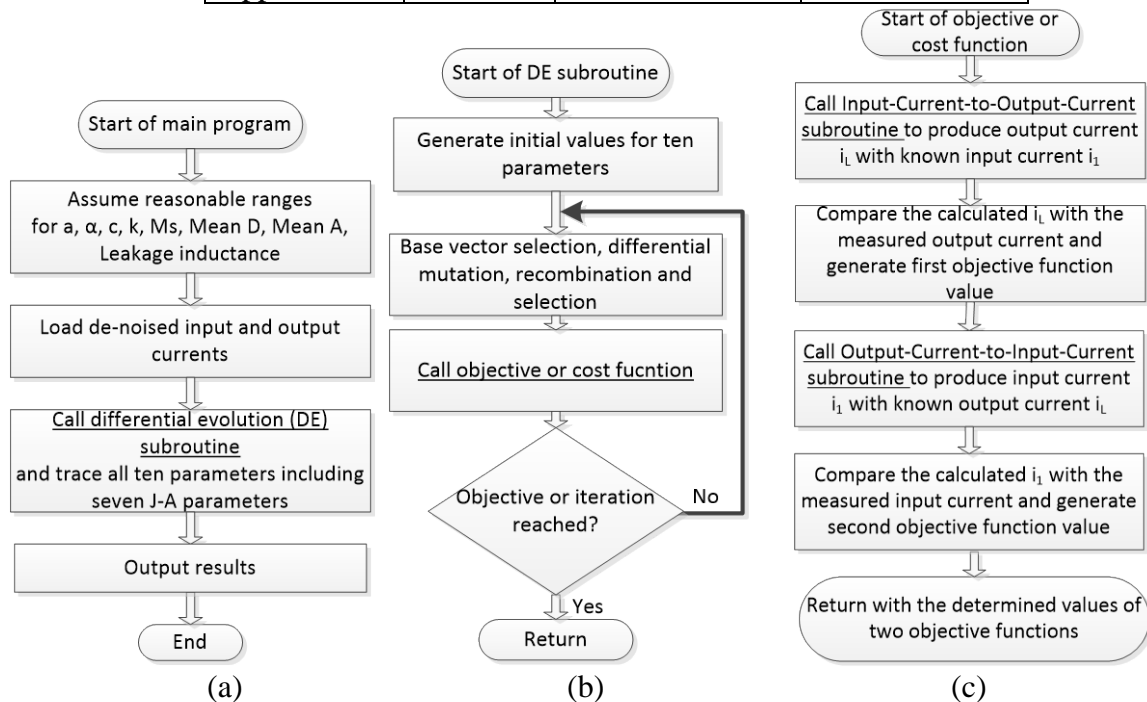


Figure 12: (a) Flowchart of main program; (b) Flowchart of differential evolution algorithm; (c) Flowchart of objective function

To verify the validity of the identified parameters, more calculation has been done. Figure 15 shows a different level of magnetization with the burden of 2.2 Ω . One can see from it that with the input current given, the traced output currents agree well with the measured values. Absolute differences between the traced and measured output currents, and between measured input current divided by CT ratio and measured output current in this case and corresponding percentage difference are shown in Fig. 16. The percent values in Fig. 16 were calculated by using maximum of the measured output current, which occurs around 0.024 s as shown in the right-hand-side graph of Fig. 15. From Fig. 16 one can see that the error with compensation or from the traced one is very small. In contrast without compensation the error is significant and can be as high as 18%. This shows the validity of developed method and necessity of compensation. Nevertheless the compensation is not perfect. Further improvement will be done in the future.

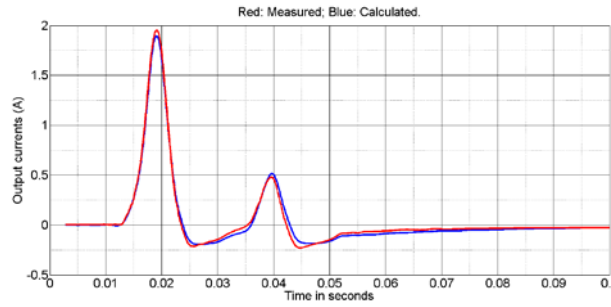


Figure 13: Measured output currents used for parameters’ extraction with a burden of 2.2Ω and its calculated output current with the identified parameters

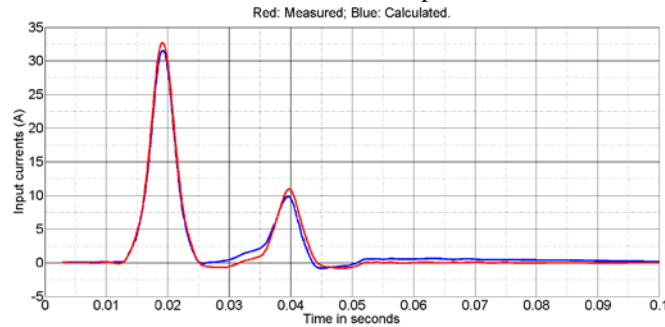


Figure 14: Measured input currents used for parameters’ extraction with a burden of 2.2Ω and the calculated input current with the identified parameters

Table 2A: Lower and upper limit of parameters in J-A model

| Parameter | a A/m | α 1E-3 | c | K_0 A/m | K_I A/m | σ | M_s kA/m |
|-------------------|------------|------------------|------|--------------|--------------|----------|---------------|
| Identified values | 1089 | 0.60 | 0.55 | 454 | 83.1 | 400.1 | 1430 |

Table 2B: Lower and upper limit of parameters for dimensions and leakage inductance

| Parameter | Mean length (cm) | Mean cross section (cm^2) | Leakage inductance (mH) |
|-------------------|---------------------|---|----------------------------|
| Identified values | 6.35 | 6.77 | 12.24 |

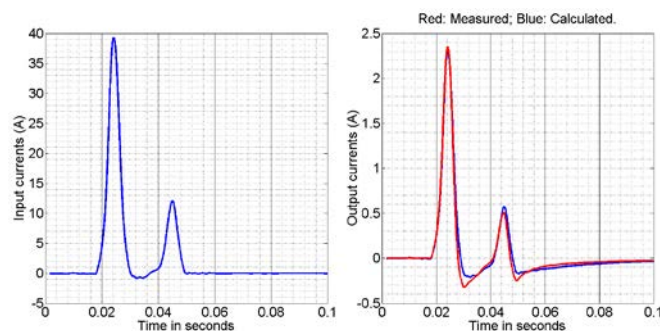


Figure 15: Calculation of output current with known input current and a burden of 2.2Ω

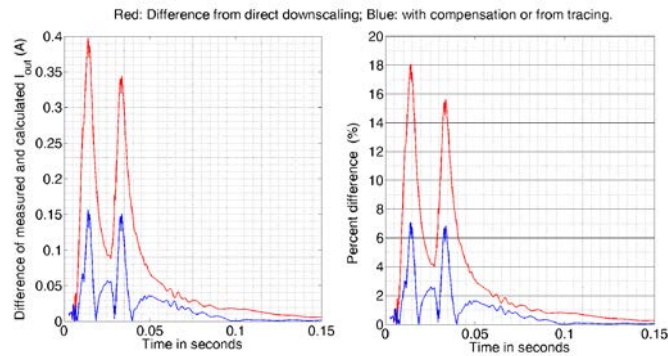


Figure 16: Difference of traced and measured output currents: Left – absolute difference; Right – Percent difference with respect to maximum measured output current; Red – Difference of measured input current divided by CT ratio and measured output current; Blue: Difference between traced and measured output current.

Figures 17 and 18 are the verification at a burden of 1.2Ω , in which the input current is as high as 50 A. Again one can see that measured and calculated currents agree well.

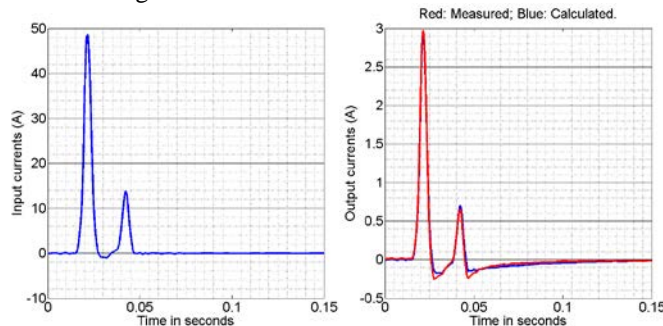


Figure 17: Calculation of output current with known input current and a burden of 1.2Ω

Figures 19 and 20 show the verification at another burden of 0Ω , in which the input current is as high as 110 A. That is to say, the secondary side of the CT is short-circuited. From these two figures, one can again see that measured and calculated currents agree well with the identified parameters.

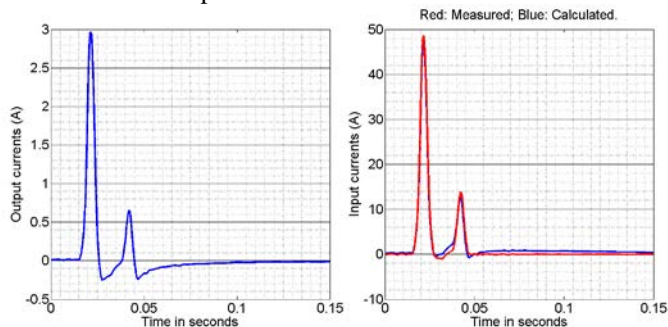


Figure 18: Calculation of input current with known output current and a burden of 1.2Ω

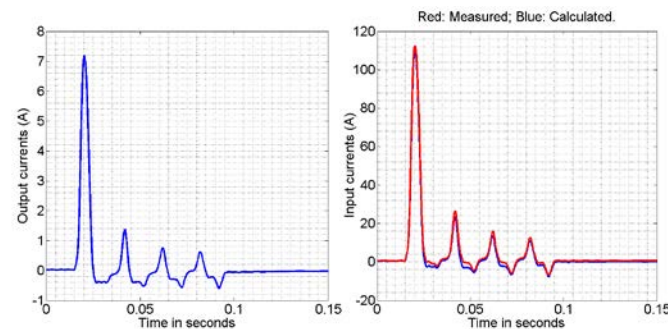


Figure 19: Calculation of input current with known output current and a burden of 0Ω

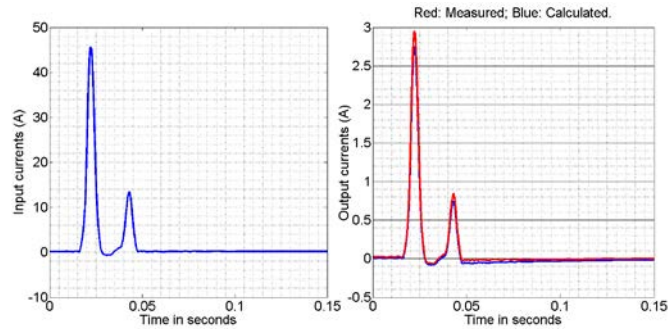


Figure 20: Calculation of output current with known input current and a burden of 0Ω

To have a further examination on the validity of the proposed algorithms, a nearly sinusoidal current was applied to the primary side of current transformer under test and the secondary side burden is 19Ω . The reason that 19Ω burden was adopted is to make saturation happen with smaller primary side and secondary side currents. Figure 21 shows the measured primary side current referred to secondary side and measured secondary side current, from which one can see that there is a pronounced difference between them. Furthermore the secondary side current presents clear saturation. With the measured secondary side current as shown in Fig. 21, the compensation algorithm as shown in Fig. 4 was implemented to calculate the magnetizing current with the extracted parameters as shown in Table II. The calculated magnetizing current is shown in Fig. 22 and was added to the measured secondary side current to fulfil compensation purpose. The compensated current is shown in Fig. 23, where the measured primary side current referred to secondary side is also shown. From the two graphs in Fig. 23, one can see that compensated secondary current is very close to the measured primary side current referred to the secondary side. This validates the effectiveness of the proposed method.

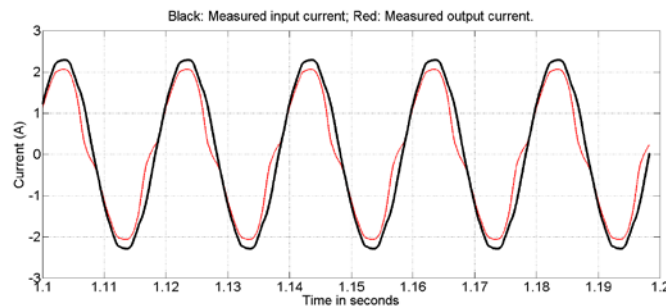


Figure 21: Measured input current referred to secondary side of CT and measured output current

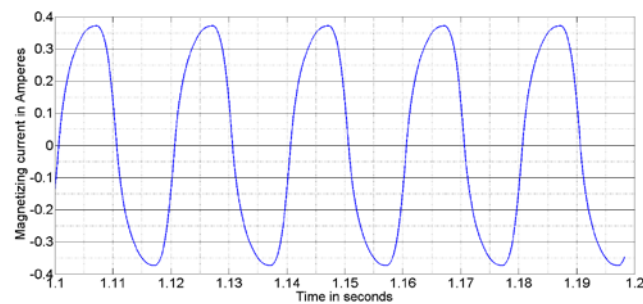


Figure 22: Calculated magnetizing current with measured output current and extracted parameters in Table 2

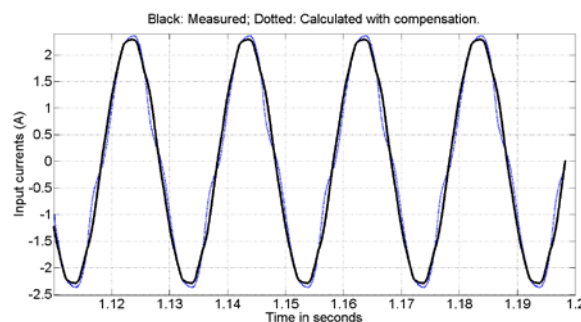


Figure 23: Measured and compensated input currents referred to secondary side

As the CT under test is sealed in resin, its core dimensions are unknown. Putting these dimensions as unknowns and identifying them successfully is one of major contributions by this paper. Nevertheless, if one knows dimensions of current transformers, the proposed method will make the parameter identification much easier.

Although the pulsating current is produced to characterize a conventional magnetic-cored current transformer, it can be used to characterize optical current transformer also. To characterize current transformers with much larger ratings, one may scale up the circuit by reducing the rated secondary side voltage of 240V/18V transformer and value of inductance L1 as shown in Fig. 5.

6. CONCLUSION

This paper presents a method for identifying parameters in the Jiles-Atherton model for commercial current transformers using pulsating inrush current source and differential evolution algorithm. The pulsating inrush current is generated from a switched circuit with an inductor load. As the peak inrush current can be as high as 20 times its steady-state values flowing through the inductor, such generated large current is suitable for characterizing commercial CTs with large ratings. Furthermore the inrush current is closer to fault current soon after fault occurs than sinusoidal waveform. To demonstrate such method, an CT has been adopted in the experiment. Besides the parameters in the Jiles-Atherton model, the effective dimensions of the CT including mean length and mean cross section and leakage inductance have been chosen as the unknowns to be identified as well. It is found that the proposed method is effective in tracing and identifying all the unknowns through differential evolution algorithm. Nevertheless careful de-noising of the measured input and output current is a pre-condition for success. To fulfil this purpose, wavelet transform has been adopted. A proper selection of current level for parameter identification must be observed as well. The generated pulsating inrush current is also suitable for characterizing the performance of optical current transformers. The proposed method can be modified to fulfil CT compensation purpose for protection system to operate properly, especially under severe fault conditions, where the measured current at the secondary side could depart tremendously from the downscaled primary side current. This is our future work.

7. REFERENCES

- [1]. SadikKucuksari, and George G.Karady, "Experimental Comparison of Conventional and Optical Current Transformers", IEEE Trans. Power Del., vol. 25, no. 4, pp. 2455-2463, 2010.
- [2]. Kondrath, Nisha; Kazimierczuk, Marian K., "Bandwidth of Current Transformers", IEEE Trans. Instrum. Meas., vol. 58, no. 6, pp. 2008-2016, 2009.
- [3]. Firouz Badrkhani Ajaei, Majid Sanaye-Pasand, Mahdi Davarpanah, Afshin Rezaei-Zare, and Reza Iravani, "Compensation of the Current-Transformer Saturation Effects for Digital Relays", IEEE Trans. Power Del., vol. 26, no. 4, pp. 2531-2540, 2011.
- [4]. L. Dalessandro and A. Ferrero, "A Method for the Determination of the Parameters of the Hysteresis Model of Magnetic Materials", IEEE Trans. Instrum. Meas., vol. 43, no. 4, pp. 599-605, AUG 1994.
- [5]. Sy-Ruen Huang, Hong-Tai Chen, Chueh-Cheng Wu, Chau-Yu Guan, and Chiang Cheng, "Distinguishing Internal Winding Faults From Inrush Currents in Power Transformers Using Jiles-Atherton Model Parameters Based on Correlation Coefficient", IEEE Trans. Power Del., vol. 27, no. 2, pp. 548-553, 2012.
- [6]. Shun-Tsai Liu, Sy-Ruen Huang, Hung-Wei Chen, Ting-Yen Hsien, "Current Transformer Module Basing the Jiles-Atherton Hysteresis Model in EMTP/ATP Simulation", IPEC: International Power Engineering Conference, Vols 1 and 2 Pages: 653-656, Published: 2005.
- [7]. Ali Hooshyar and Majid Sanaye-Pasand, "CT Saturation Detection Based on Waveform Analysis Using a Variable-Length Window", IEEE Trans. Power Del., vol. 26, no. 3, pp. 2040-2-50, 2011.
- [8]. N. Locci and C. Muscas, "A digital compensation method for improving current transformer accuracy", IEEE Trans. Power Del., vol. 15, no. 4, pp. 1104-1109, Oct. 2000.
- [9]. Y. C. Kang, U. J. Lim, S. H. Kang, and P. A. Crossley, "Compensation of the distortion in the secondary current caused by saturation and remanence in a CT", IEEE Trans. Power Del., vol. 19, no. 4, pp. 1642-1649, Oct. 2004.
- [10]. X. Wang, D. W. P. Thomas, M. Sumner, J. Paul, and S. H. L. Cabral, "Characteristics of Jiles-Atherton Model Parameters and Their Application to Transformer Inrush Current Simulation", IEEE Trans. Magn., vol. 44, no. 3, pp. 340-345, 2008.
- [11]. D.M Zhang, K.J. Tseng and Y.T. Liu, "Study on Inrush Current Phenomenon in DC-DC Converter with Isolating Transformer", AUPEC New Zealand, 2010.
- [12]. D.C. Jiles, "Frequency Dependence of Hysteresis Curves in Non-conducting Magnetic Materials", IEEE Trans. Magn., vol. 29, pp. 3490-3492, 1993.
- [13]. D. C. Jiles, "A self consistent generalized model for the calculation of minor loop excursions in the theory of hysteresis", IEEE Trans. Magn., vol. 28, pp. 2602-2604, 1992.
- [14]. D.M.Zhang, and Fletcher John, "Double-Frequency Method Using Differential Evolution for Identifying Parameters in the Dynamic Jiles-Atherton Model of Mn-Zn Ferrites", IEEE Trans. Instrumentation and Measurement, vol. 62, no. 2, pp. 460-466, 2013.

- [15]. V. Kenneth, Price, Rainer M. Storn, Jouni A. Lampinen, *Differential Evolution – A Practical Approach to Global Optimization, Natural Computing Series*, Springer, 2005.
- [16]. Anyong Qing, *DIFFERENTIAL EVOLUTION -Fundamentals and Applications in Electrical Engineering*, John Wiley & Sons Pte Ltd, 2009.
- [17]. S. G. Mallat, "Time Meets Frequency", in *A Wavelet Tour of Signal Processing : The Sparse Way*, Sparse ed Amsterdam ; Boston: Elsevier /Academic Press, pp. 89-150, 2009.
- [18]. S. G. Mallat, "Denoising", in *A Wavelet Tour of Signal Processing : The Sparse Way*, Sparse ed Amsterdam ; Boston: Elsevier /Academic Press, pp. 535-606, 2009.